View metadata, citation and similar papers at core.ac.uk
brought to you by CORE
provided by Directory of Open Access Journals

Eurasian Chemico-Technological Journal 20 (2018) 255-262

https://doi.org/10.18321/ectj758

Numerical and Experimental Investigation of Laminar One-Dimensional Counter-Flow Flames Using Product Gas From Pyrolysis and Gasification of Woody Biomass

M.-T. Scharl*, D.A. Greenhalgh, A. Dieguez-Alonso, F. Behrendt

Technische Universität Berlin, Institute of Energy Engineering, Fasanenstr. 89, 10623 Berlin, Germany

Article info

Received:
20 January 2018

Received in revised form:
18 April 2018

Accepted:
19 May 2018

Abstract

Further advances in the utilization of biomass-based gaseous fuels in combustion systems require a deeper understanding of the combustion chemistry behind, as well as of the coupling of the chemistry with physical phenomena such as turbulence. The former is investigated in the present study combining both experiments with numerical simulations of different types of laminar non-premixed flames (sooting and non-sooting) in a counter-flow setup. The focus is put on synthetic gas mixtures, resembling, to different extents, typical compositions of the product gas obtained in biomass gasification consisting of CH_4 (reference) and CH_4 mixed with CO_2, N_2, O_2, and/or H_2, always. The oxidizer in all cases is air. A wide range of air-fuel ratios is considered. The influence of the product gas composition on the flame behaviour and flame structure with respect to the changes of the species profiles and peak temperatures with changing flow velocities is discussed. Laser-based spectroscopy techniques, in particular laser-induced Rayleigh scattering and laser-induced fluorescence (LIF), are applied as diagnostic tools. The former can provide an accurate understanding of temperature distributions, while the latter helps to identify the flame front through the tracking of intermediate species, such as CH_2O (formaldehyde). Additionally, CH* chemiluminescence contributes to localize the flame front. Lastly, the influence of the N_2-shroud flow velocities and diameters, as well as resulting buoyancy effects due to a raise in temperature, are taken into account. In correspondence to these experiments, the flames are numerically simulated by an in-house time-dependent implicit Fortran code.

1. Introduction

Thermochemical conversion is a promising alternative for decentralized energetic utilization of biomass and waste. In particular, processes such as pyrolysis and gasification offer the possibility to produce a fuel gas to be used, among other applications, in internal combustion engines or turbines as part of combined heat and power generation (CHP). However, these fuels are more complex than conventional gaseous fuels regarding their composition depending on the conversion process and conditions. Despite the low calorific value and possible low quality of biomass and organic residues, this feedstock has increased its appeal due the essentially unlimited availability [1, 2]. The varying composition of the input materials and the wide range of possible process conditions do result in significantly different product gas compositions. The subsequent combustion process has to deal with significant amounts of diluents like CO_2 and N_2, next to combustible species like H_2, CH_4 and CO [3]. In the present work the influence of the product gas composition on the flame behaviour and flame structure is addressed.

Investigation on syngas diffusion flames has been widely addressed in literature, with focus on the combustion of individual syngas components [4], hydrogen fuels [5] airstream dilution [6], the influence of primarily CO_2 dilution [7] or methane-air diffusion flames in a counter-flow setup [8]. In this study experiments and numerical simulation on laminar counter-flow diffusion flames are combined. The understanding of the combustion behaviour of these complex gaseous fuels in such flames is essential for the further application of the

*Corresponding author. E-mail: m.scharl@tu-berlin.de

© 2018 Al-Farabi Kazakh National University

laminar flamelet model to describe turbulent combustion [8]. The flamelet model describes the flame front as a collective of individual laminar flame elements in a turbulent flow profile, providing an approach to describe these flames.

In the present study, the laminar diffusion flames were numerically simulated by an in-house implicit Fortran code [9], which solves the governing equations for total mass, mass fractions, momentum and energy for non-stationary laminar one-dimensional flames. In the simulations about 80 species were taken into account with a reaction mechanism of more than 500 elementary reversible reactions [10].

Regarding the experimental investigation, laser-induced Rayleigh scattering was applied to measure the temperature profile in the flame. This approach avoids potential perturbations of contact probes like thermocouples on the flame and contributes to a more accurate diagnosis. This is of special relevance in these investigations due to the impact of temperature on reaction rates and pollutant levels [11]. The Rayleigh intensity depends on the gas species scattering cross section and, therefore, also on the mixture fraction at each location in the flame. The cross section is temperature-dependant, being negatively correlated to temperature. This leads to different cross sections and hence scattering intensities in the flame profile in the wings and the centre of the flame.

This change in scattering intensity is shown in Fig. 1 for three flames excited at λ = 532 nm, using three flow velocities (20 cm s^{-1}, 40 cm s^{-1} and 60 cm s^{-1}) and the same fuel composition.

CH_2O is an important intermediate species in combustion, typically used to investigate the flame structure. In the present work, laser-induced fluorescence is used as a non-intrusive technique to allow a sensitive detection of CH_2O with an excitation wavelength of λ = 355 nm [12, 13]. CH* chemiluminescence is also used to locate the main heat release zone in a flame [14]. In this study, CH* chemiluminescence at λ = 430 nm is collected to determine the spatial position of the flame between the two nozzles.

2. Experimental

A schematic of the experimental set-up is shown in Fig. 2. The burner system consists of two opposed nozzles, each 24.8 mm in diameter, with a varying separation distance. To achieve the compromise of having a stable laminar flame and also reducing the reflections induced by the laser light on the nozzles, an axial distance of 18.9 mm was used for all experiments presented here. The inner jets of oxidizer and fuel are both surrounded by an annular co-flow of N_2 to avoid perturbations from ambient air and, therefore, ensure stabilization. By using a water-cooled heat exchanger at ambient temperature, the upper part of the burner assembly was cooled down.

The excitation wavelengths for laser-induced Rayleigh scattering (λ = 532 nm) and laser-induced fluorescence of CH_2O (λ = 355 nm) were generated by means of the second and third harmonics of a Quanta-Ray Lab pulsed Nd:YAG laser (Model: Lab150 by Spectra Physics, Santa Clara, USA). The laser beam was guided via periscopes into a focusing spherical lens, subsequently forming the beam into a thin collimated sheet (9 mm) by a combination of diverging and converging cylindrical lenses. The laser sheet entered the measurement region between the nozzles of the counter-flow burner, being imaged by an intensified CCD camera (Model: Nanostar by LaVision, Göttingen, Germany) positioned perpendicular to the laser sheet to collect the signal. By a linear response to the signal this ICCD is able to acquire and store hundreds of single shot images, using a chip size of 1280 × 1024 pixels. The wavelength-specific

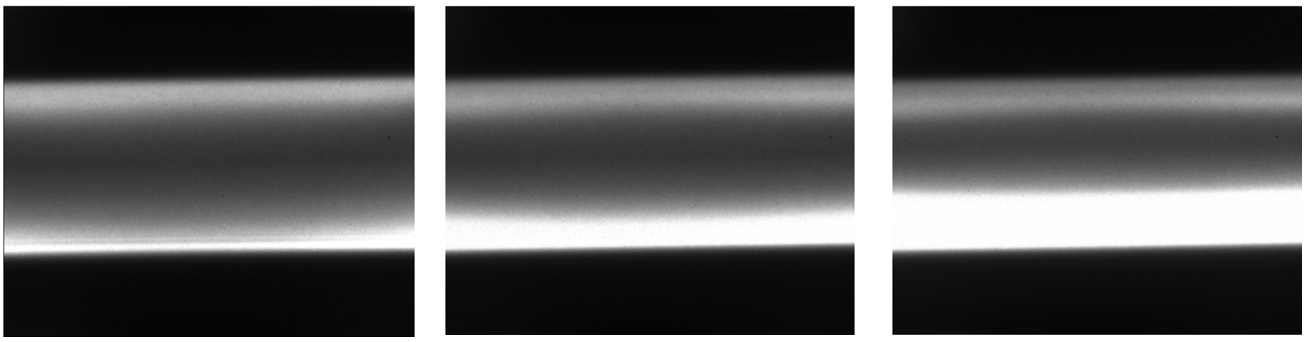

Fig. 1. Rayleigh signal (corresponding to temperature fields for diluted non-premixed CH_4 – N_2 – CO_2 – air flames (top: air side; bottom: fuel side); at velocities of 20 cm s^{-1}, 40 cm s^{-1} and 60 cm s^{-1} (left to right).

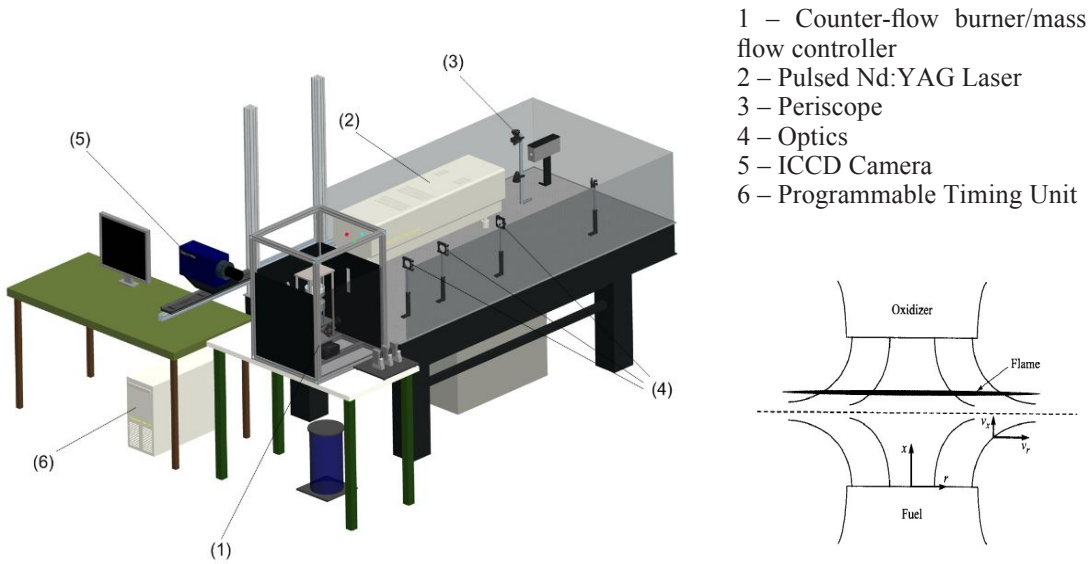

Fig. 2. Schematic of the experimental set-up (left) and counter flow flame (right) [15].

signals (scattering, fluorescence, chemiluminescence) was collected using BrightLine single-band bandpass (notch) filters, allowing only the respective wavelengths regions to pass through. All images obtained were corrected pulse by pulse via an energy monitor (Model: V9 dual head by LaVision, Göttingen, Germany) and for background scatter and variations in the laser sheet intensity.

Two compositions of gaseous fuel at velocities of 20 cm s^{-1}, 40 cm s^{-1} and 60 cm s^{-1} were chosen for the experimental and numerical studies. Both fuel-side compositions contained 40% (volume) CH_4 and 60% of diluent with the diluent being: a) 40% CO_2 and 20% N_2 or b) 20% CO_2 and 40% N_2. Moreover, the addition of 5% H_2 or up to 8% O_2 to the fuel was investigated. The gases were mixed via mass-flow controllers (Model: red-y by Vögtlin, Aesch, Switzerland). The gas mixtures are presented in Table 1.

In each study the experiments were conducted at identical velocities for the fuel- and oxidizer-sides. The flame is always located on the airside with respect to the stagnation plane. Increasing flow velocities, in the limit, leads to aerodynamic quenching of the flame. This extinction point can be identified by tracing the maximum temperature as function of the strain rate. The higher this critical strain rate, the higher its resilience to quenching, making the flame more stable for a wider range of flow conditions. That is desirable for an industrial combustion system, since the turn down ratio of the burner could be therefore increased, allowing a wider range of firing rates and thus enhancing the flexibility of the system.

Table 1
Compositions of investigated fuels

Fuel composition	CH_4 [vol-%]	CO_2 [vol-%]	N_2 [vol-%]	H_2 [vol-%]	O_2 [vol-%]
Case A	40	40	20	-	-
Case A – H_2 addition	38	38	19	5	-
Case A – O_2 addition	39.2	39.2	19.6	-	2
Case A – O_2 addition	38.4	38.4	19.2	-	4
Case A – O_2 addition	37.6	37.6	18.8	-	6
Case A – O_2 addition	36.8	36.8	18.4	-	8
Case B	40	20	40	-	-
Case B – H_2 addition	38	19	38	5	-
Case B – O_2 addition	39.2	19.6	39.2	-	2
Case B – O_2 addition	38.4	19.2	38.4	-	4
Case B – O_2 addition	37.6	18.8	37.6	-	6
Case B – O_2 addition	36.8	18.4	36.8	-	8

The total Rayleigh scattering signal collected by a detector can be written as follows [11]

$$S = \eta I N V \int_{\Delta\Omega} \left(\frac{\delta\sigma}{\delta\Omega}\right)_{mix} \delta\Omega \qquad (1)$$

where V is the observation volume, N the number density, I the incident laser intensity, η the optical collection efficiency, $(\delta\sigma/\delta\Omega)_{mix}$ the differential scattering cross section of the gas mixture and $\Delta\Omega$ the solid angle subtended by the collection optics. For a single molecular species at a specific wavelength the total Rayleigh scattering cross section can be written as follows [10]

$$\sigma(\lambda) = \frac{24\pi^3}{\lambda^4 N^2}\left(\frac{n(\lambda)^2 - 1}{n(\lambda)^2 + 2}\right)^2 \left(\frac{6 + 3\rho_0(\lambda)}{6 - 7\rho_0(\lambda)}\right) \qquad (2)$$

where N is the number density, $n(\lambda)$ is the refractive index and $\rho_0(\lambda)$ is the depolarization ratio. Our approach to analysis follows that of Connelly et al. [16] where the directly measured Rayleigh scattering is compared with a model of the Raleigh scattering rather than an interpolation of the Rayleigh to estimate temperature or density that introduces errors which cannot be easily quantified [16]. Furthermore, based on the simulated species profiles and the incorporation of the scattering Rayleigh cross sections of the major species, together with the imaging systems possible point spread function to minimize crosstalk background phenomena, a good fit between model and experiment can be established. All contributions to background arising from scattering and the point spread function of the CCD need therefore to be included when analysing the experimental measurements and comparing them with the numerical results of the corresponding flames and vice versa [16].

3. Results

The numerical and experimental results regarding the Rayleigh scattering and subsequently extracted temperature curves (based on [11]) at fuel side variations of 40% CH_4 and a diluent distribution of either 40% CO_2 and 20% N_2 (case A) or 20% CO_2 and 40% N_2 (case B) at velocities of 20 cm s^{-1} and 60 cm s^{-1} are shown in Fig. 3.

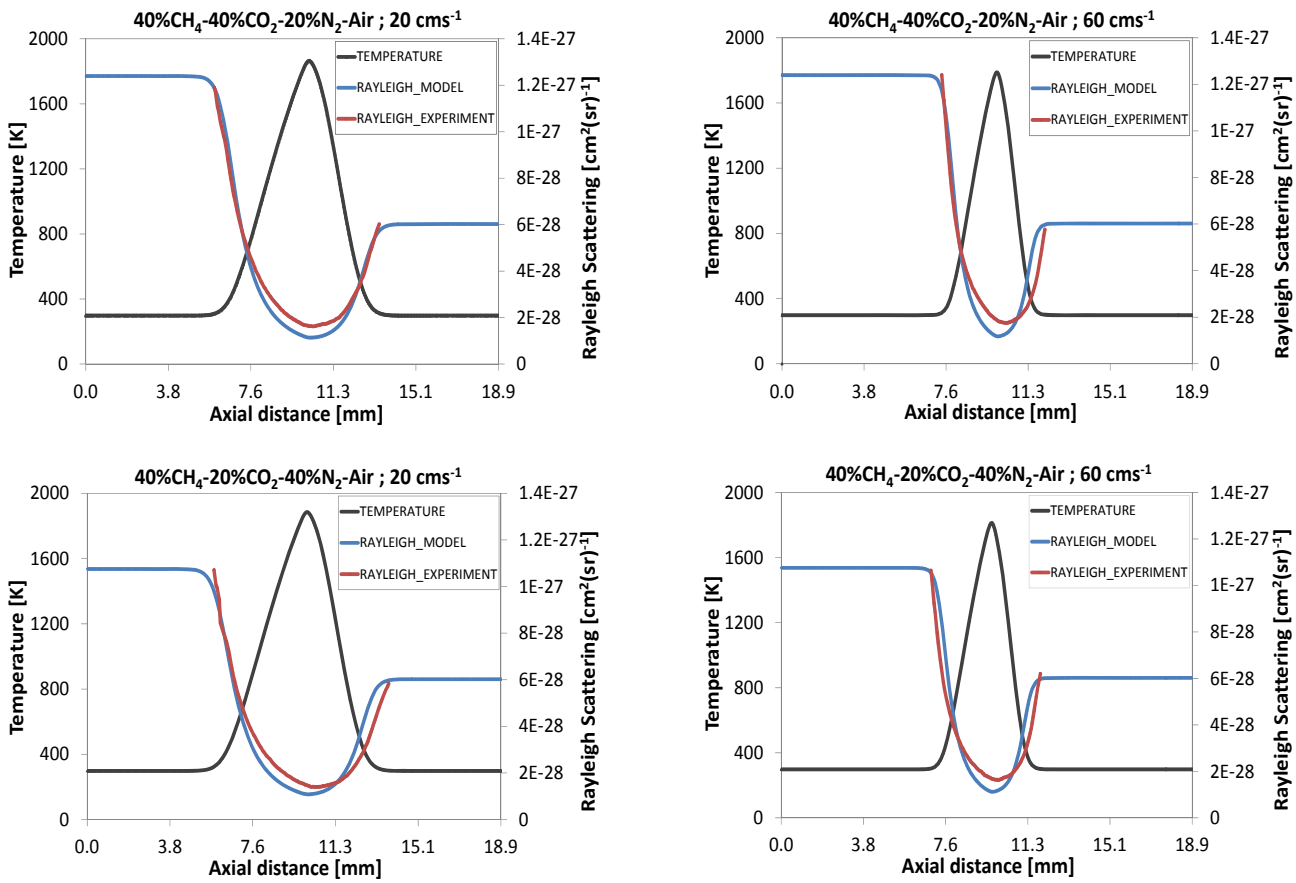

Fig. 3. Experimental and numerical solutions for 40% CH_4 – 40% CO_2 – 20% N_2 – air (case A) at 20 cm s^{-1} (top left) and 60 cm s^{-1} (top right); 40% CH_4 –20% CO_2 – 40% N_2 – air (case B) at 20 cm s^{-1} (bottom left) and 60 cm s^{-1} (bottom right).

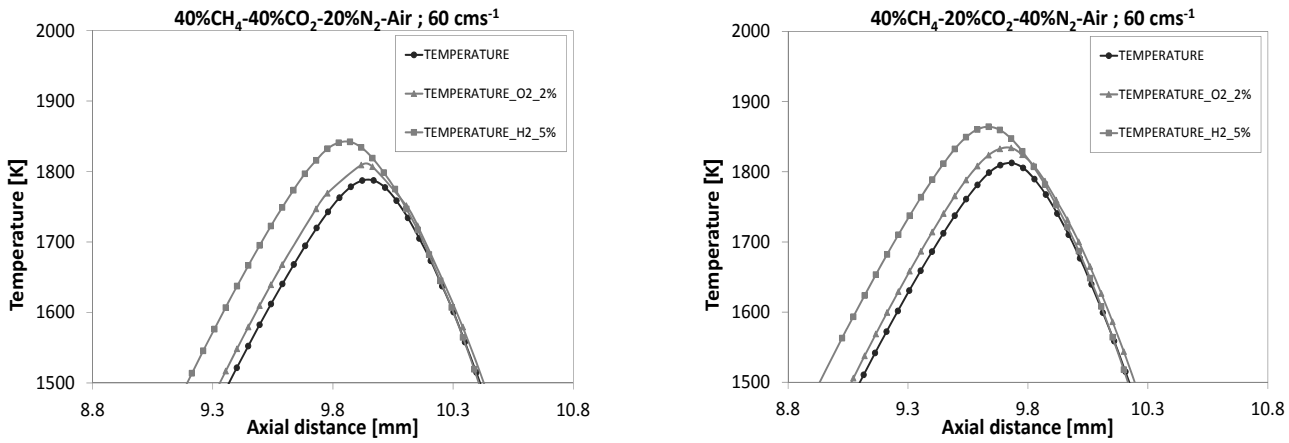

Fig. 4. Numerical solutions for temperature change in 40% CH_4 – 40% CO_2 – 20% N_2 – air (case A) flames with an addition of 2% O_2 or 5% H_2 at 60 cm s^{-1} (left) and 40% CH_4 – 20% CO_2 – 40 % N_2 – air (case B) flames with an addition of 2% O_2 or 5% H_2 at 60 cm s^{-1} (right).

The modelled profiles of the Rayleigh scattering are being compared to the experimental ones measured for each flame. There is a good agreement between numerical and experimental results. When regarding the values for the differential scattering cross sections for the gases in these fuels [11] a factor of 2.38 can be derived between the cross sections of CO_2 and N_2, this leading to the higher initial Rayleigh scattering on the fuel side (at axial distance 0–5.5 mm) for case A in comparison to case B. The initial Rayleigh scattering on the side of the oxidizer (at axial distance 13.8–18.9 mm) is equal in all cases, since air was introduced as oxidizer in all regarded studies. Towards the centre of the flame, where the peak temperatures are achieved, the scattering decreases markedly, due to the temperatures influence on the density of the gases.

The maximum temperatures at both 20 cm s^{-1} and 60 cm s^{-1} in case B decreased (21 K and 23 K respectively) compared to case A. This can be traced back to both a chemical [17] and a thermal effect [5], due to the modification of the diluent composition in the fuel and also because of the lower heat capacity and higher thermal diffusivity of N_2 compared to CO_2 as a diluent. As the velocities were increased in both cases A and B from 20 to 60 cm s^{-1}, the peak temperatures decreased by 42 K and 40 K respectively, due to fewer radicals caused by shorter residence times, resulting in an incomplete flame chemistry. When increasing the velocity and therefore strain of the flame the diffusion process is limited, which leads to a shift of the flame towards the fuel side and simultaneously reduces the flames width.

Several quantities of O_2 (2, 4, 6, and 8% in volume) and 5% in volume of H_2 were added to the fuel side compositions for cases A and B. A small quantity of O_2 may appear in the product gas when using air as gasification agent during biomass gasification processes. The content of H_2 also varies strongly depending on the choice of agent.

An addition of 2% O_2 or 5% H_2 increased the peak temperatures by 1.5% and 3.5% respectively, despite the high fraction of CO_2 with a high heat capacity, according to the numerical results shown in Fig. 4. The peak temperatures of these highly diluted flames, being < 1850 K in all cases except case B without an addition, would possibly reduce a problem of thermal NO in combustion processes.

As stated the experimental determination of CH* chemiluminescence at $\lambda = 430$ nm is a simple method of detecting the region of maximum heat release and the exact physical position of the flame in order to predict unsteady combustion behaviour [18]. Concentration measurements of CH radicals are necessary for the spatial validation of flame models, as this radical exists in a thin high-temperature region [14]. The model calculates the CH radical concentration, as opposed to the experimental measurements, where the electronically excited CH* radical is being measured. This led to continuously smaller peaks in the experimental solution, compared to the numerical outcome.

In both cases for the fuel-side compositions A and B, an increase of the velocities from 20 cm s^{-1} to 60 cm s^{-1} led to an increase of CH* chemiluminescence peak intensities by 25–27%. Though fuel-side compositions with the higher proportion of CO_2 added as diluent results in consistently lower

levels of CH* due to the quenching of the radicals by collision with the CO_2 molecule [19]. An addition of 2% O_2 or 5% H_2 by volume were also regarded for the velocity of 60 cm s^{-1} in both cases. The O_2 addition led to an increase of 5.2% and 6.9% of CH* for the compositions A and B respectively. The addition of H_2 resulted in an increase of 17.6% and 16.5% respectively. In case of O_2 this might be traced back to the reaction with the ethynyl radical, producing CH* and therefore CO and CO_2 [20, 21]. An addition of H_2 to these hydrocarbon fuel mixes led to an increase of CH* based on multiple formation reactions with C, CO and CHO [9].

Finally, the numerical results regarding the CH_2O are shown in Fig. 5. CH_2O is an important intermediate species in combustion, which is formed in preheating zones at the beginning of the flame front. Therefore, its presence is suited to localize early stages of combustion. The left side of Fig. 5 shows the numerical results based on the fuel-side composition A at 20 cm s^{-1} and 60 cm s^{-1} without additives and the results with an addition of 2% O_2 or 5% H_2 to the fuel at 60 cm s^{-1}. At higher velocity the addition of O_2 and especially H_2 led to a decrease in the CH_2O mole fraction.

The addition of O_2 (up to 8%) resulted in the development of a premixed rich flame in the pre-chemistry zone (Fig. 5, right plot). The CH_2O concentration increased markedly as the O_2 concentration increased and additionally, when raising the velocity and there-fore the strain rate of the flame (a). This second flame was most prominent though at low strain (~130 s^{-1}) and increasing O_2. An addition of 8%, as opposed to 2%, O_2 here led to a difference in peak temperature of 100 K, markedly extending the flammability of the system, possibly leading to a more complete combustion.

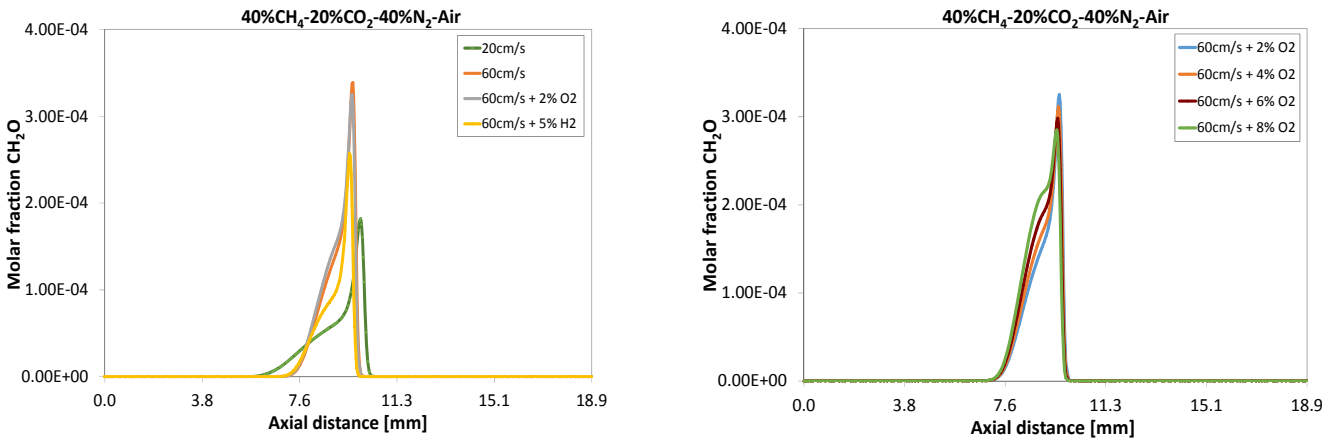

Fig. 5. Numerical results of formaldehyde molar fraction of 40% CH_4 – 20 % CO_2 – 40 % N_2 – air counter-flow flame at 20 cm s^{-1} and 60 cm s^{-1} (case A) and flames with an addition of 2% O_2 or 5% H_2 to the fuel-side at 60 cm s^{-1} (left) and 40% CH_4 – 20% CO_2 – 40% N_2 – air flame 60 cm s^{-1} with an addition of 2%, 4%, 6% and 8% of O_2 to the fuel-side (right).

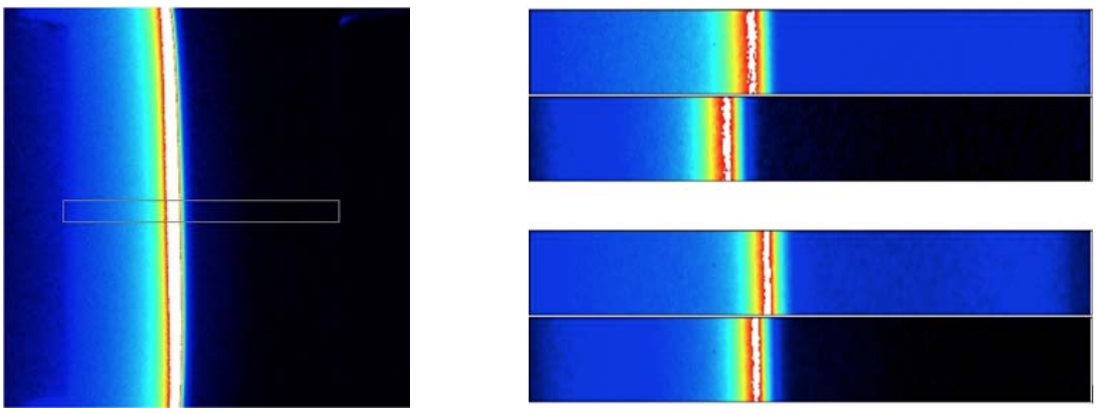

Fig. 6. Experimental CH* chemiluminescence at λCH* = 430 nm from diluted non-premixed 40% CH_4 – 60% CO_2 – air flames; left figure: highlighted centreline of flames between nozzles with rectangle, 18.89 mm long, 45 pixels high (top: air side, bottom: fuel side), right figure top: flame at $v_{air/fuel\ sides}$ = 20 cm s^{-1}, a = 41.1 s^{-1} with cold (top) and hot (bottom) nozzle on air side; right figure bot-tom: flame at $v_{air/fuel\ sides}$ = 40 cm s^{-1}, a = 82.1 s^{-1} with cold (top) and hot (bottom) nozzle on air side.

Additionally, the influence of the N_2-shroud flow (at 100% of the core jet velocities) and buoyancy effects due to a raise in temperature in the upper burner and a nozzle diameter of diameter < 25 mm were taken into account [22]. As shown in Fig. 6, the location of flames formed in a small burner (diameter = 24.7 mm) was greatly affected by buoyancy at low strains and increasing temperature. The change of temperature induced a change of the density at the oxidizer from the top nozzle. This buoyancy effect decreased at higher velocities and hence higher strain rates. The influence of the shroud flow and the buoyancy effect cannot be decoupled without further analysis [23].

4. Conclusions

This study focused on the experimental and numerical investigations of complex gaseous mixtures, similar to the ones obtained in biomass gasification, with a high content of N_2 and CO_2 as diluents next to CH_4, O_2 and H_2 as components. The investigations were carried out with counter-flow diffusion flames at low velocities and, therefore, strain. An increase of flow velocities and the thereby finally induced extinction of the diluted flames are discussed with respect to the changes of the temperature profiles and decreasing peak temperatures. Furthermore, with increasing strain rates a reduction of the flame width and the development of the CH_2O concentration as well as of radicals like CH* were analysed.

The experimental laser-induced Rayleigh scattering and the subsequently following temperature distributions were in good agreement with the numerical results. The proportions of different diluents in the composition on the fuel-side led to differing results regarding the peak temperatures at varying velocities, mostly resulting from chemical and thermal effects, based on heat capacities and thermal diffusivities. Small quantities of H_2 and O_2 had a considerable effect, not only on peak temperatures in all flames considered, but also on the molar fractions and signal intensities of CH* and CH_2O, which were also in good agreement for both the numerical and the experimental studies. The choice of the diluent also played a major role, especially with respect to flame resilience to extinction by strain. Lastly, an addition of O_2 to the fuel in smaller quantities had a great impact on the formaldehyde concentration and expanded the flammability of the system markedly with respect to strain. This would advance the possibility of the introduction of air to i.e. a gasification system, as a cheap solution for a more complete combustion system.

References

[1]. M. Dudynski, K. Kwiatkowski, K. Bajer, *Waste Manage.* 32 (2012) 685–691. DOI: 10.1016/j.wasman.2011.11.017

[2]. N. Cerone, F. Zimbardi, L. Contuzzi, E. Alvino, M. Carnevale, V. Valerio, *Fuels* 28 (2014) 3948–3956. DOI: 10.1021/ef500782s

[3]. K. Kwiatkowski, E. Mastorakos, *Energy Fuels* 30 (6) (2016) 4386–4397 DOI: 10.1021/acs.energyfuels.5b02580

[4]. A.B. Sahu, R.V. Ravikrishna, *Combust. Flame* 173 (2016) 208–228. DOI: 10.1016/j.combustflame.2016.09.003

[5]. H. Xu, F. Liu, S. Sun, Y. Zhao, S. Meng, W. Tang, *Combust. Flame* 177 (2017) 67–78. DOI: 10.1016/j.combustflame.2016.12.001

[6]. D.E. Giles, S. Som, S.K. Aggarwal, *Fuel* 85 (2006) 1729–1742. DOI: 10.1016/j.fuel.2006.01.027

[7]. C.A. Hoerlle, L. Zimmer, F.M. Pereira, *Fuel* 203 (2017) 671–685. DOI: 10.1016/j.fuel.2017.04.049

[8]. R.V. Ravikrishna, A.B. Sahu, *Int. J. Spray Combust.* 10 (2017) 38–71. DOI: 10.1177/1756827717738168

[9]. G. Dixon-Lewis, T. David, P.H. Gaskell, S. Fukutani, H. Jinno, J.A. Miller, R.J. Kee, M.D. Smooke, N. Peters, E. Effelsberg, J. Warnatz, F. Behrendt, *P. Combust. Inst.* 20 (1) (1985) 1893–1904. DPO: 10.1016/S0082-0784(85)80688-3

[10]. R.J. Kee, J.A. Miller, J. Warnatz, A Fortran computer code package for the evaluation of gas phase viscosities, conductivities and diffusion coefficients. Sandia National Laboratories Report SAND83-8209 (1983).

[11]. G. Sutton, A. Levick, G. Edwards, D. Greenhalgh, *Combust. Flame* 147 (2006) 39–48 (2006). DOI: 10.1016/j.combustflame.2006.07.013

[12]. S. Bejaoui, X. Mercier, P. Descroux, E. Therssen, *Combust. Flame* 161 (2014) 2479–2491. DOI: 10.1016/j.combustflame.2014.03.014

[13]. A. Burkert, W. Paa, M. Reimert, K. Klinkov, C. Eigenbrod, *Fuel* 111 (2013) 384–392. DOI: 10.1016/j.fuel.2013.03.041

[14]. P. Nau, J. Krüger, A. Lackner, M. Letzgus, A. Brockhinke, *Appl. Phys. B* 107 (3) (2012) 551–559. DOI: 10.1007/s00340-012-5006-9

[15]. S. Turns, An Introduction to Combustion: Concepts and Applications. McGraw-Hill (2012).

[16]. B.C. Connelly, B.A.V. Bennett, M.D. Smooke, M.B. Long, *P. Combust. Inst.* 32 (2009) 879–886. DOI: 10.1016/j.proci.2008.05.066

[17]. F. Liu, A.E. Karatas, Ö.L. Gülder, M. Gu, *Combust. Flame* 162 (2015) 2231–2247. DOI: 10.1016/j.combustflame.2015.01.020

[18]. D. Giassi, S. Cao, B.A.V. Bennett, D.P. Stocker, F. Takahashi, M.D. Smooke, M.B. Long, *Combust. Flame* 167 (2016) 198–206. DOI: 10.1016/j.combustflame.2016.02.012

[19]. T. Garcia-Armingol, J. Ballester, *Int. J. Hydrogen Energ.* 39 (2014) 20255–20265. DOI: 10.1016/j.ijhydene.2014.10.039

[20]. M. De Leo, A. Saveliev, L.A. Kennedy, S.A. Zelepouga, *Combust. Flame* 149 (2007) 435–447. DOI: 10.1016/j.combustflame.2007.01.008

[21]. G.P. Smith, C. Park, L.A. Kennedy, J. Luque, *Combust. Flame* 140 (2005) 385–389. DOI: 10.1016/j.combustflame.2004.11.011

[22]. C.B. Oh, E. Ju Lee, J. Park, *Int. J. Spray Combust.* 2 (3) (2010) 199–218. DOI: 10.1260/1756-8277.2.3.199

[23]. L. Figura, A. Gomez, *Combust. Flame* 159 (2012) 142–150. DOI: 10.1016/j.combustflame.2011.06.013